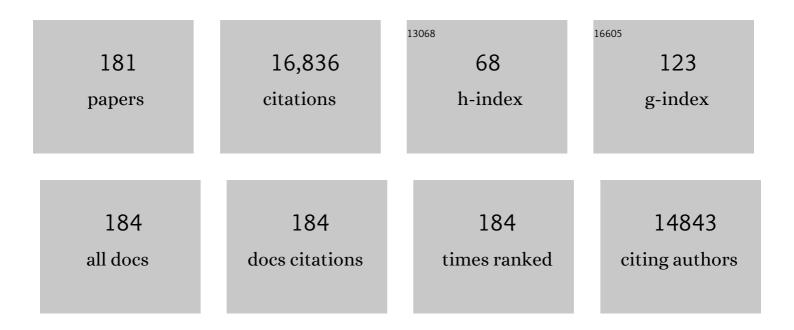
List of Publications by Year in descending order

Source: https://exaly.com/author-pdf/6473177/publications.pdf Version: 2024-02-01



SHIRO XI

#	Article	IF	CITATIONS
1	Single Cobalt Atoms Anchored on Porous N-Doped Graphene with Dual Reaction Sites for Efficient Fenton-like Catalysis. Journal of the American Chemical Society, 2018, 140, 12469-12475.	6.6	1,044
2	Chemical and structural origin of lattice oxygen oxidation in Co–Zn oxyhydroxide oxygen evolution electrocatalysts. Nature Energy, 2019, 4, 329-338.	19.8	977
3	Iron-facilitated dynamic active-site generation on spinel CoAl2O4 with self-termination of surface reconstruction for water oxidation. Nature Catalysis, 2019, 2, 763-772.	16.1	678
4	<i>In Situ</i> Raman Spectroscopy of Copper and Copper Oxide Surfaces during Electrochemical Oxygen Evolution Reaction: Identification of Cu ^{III} Oxides as Catalytically Active Species. ACS Catalysis, 2016, 6, 2473-2481.	5.5	592
5	A Grapheneâ€Supported Singleâ€Atom FeN ₅ Catalytic Site for Efficient Electrochemical CO ₂ Reduction. Angewandte Chemie - International Edition, 2019, 58, 14871-14876.	7.2	410
6	Enlarged CoO Covalency in Octahedral Sites Leading to Highly Efficient Spinel Oxides for Oxygen Evolution Reaction. Advanced Materials, 2018, 30, e1802912.	11.1	338
7	Metal Atomâ€Doped Co ₃ O ₄ Hierarchical Nanoplates for Electrocatalytic Oxygen Evolution. Advanced Materials, 2020, 32, e2002235.	11.1	332
8	A Flexible Microwave Shield with Tunable Frequencyâ€Transmission and Electromagnetic Compatibility. Advanced Functional Materials, 2019, 29, 1900163.	7.8	299
9	Copper Single Atoms Anchored in Porous Nitrogen-Doped Carbon as Efficient pH-Universal Catalysts for the Nitrogen Reduction Reaction. ACS Catalysis, 2019, 9, 10166-10173.	5.5	284
10	Covalency competition dominates the water oxidation structure–activity relationship on spinel oxides. Nature Catalysis, 2020, 3, 554-563.	16.1	284
11	Scalable two-step annealing method for preparing ultra-high-density single-atom catalyst libraries. Nature Nanotechnology, 2022, 17, 174-181.	15.6	279
12	Low-Crystalline Bimetallic Metal–Organic Framework Electrocatalysts with Rich Active Sites for Oxygen Evolution. ACS Energy Letters, 2019, 4, 285-292.	8.8	255
13	Tailoring the Co 3d-O 2p Covalency in LaCoO ₃ by Fe Substitution To Promote Oxygen Evolution Reaction. Chemistry of Materials, 2017, 29, 10534-10541.	3.2	254
14	Exceptionally active iridium evolved from a pseudo-cubic perovskite for oxygen evolution in acid. Nature Communications, 2019, 10, 572.	5.8	254
15	Spinâ€Related Electron Transfer and Orbital Interactions in Oxygen Electrocatalysis. Advanced Materials, 2020, 32, e2003297.	11.1	240
16	Identification of the Electronic and Structural Dynamics of Catalytic Centers in Single-Fe-Atom Material. CheM, 2020, 6, 3440-3454.	5.8	231
17	Activating and Optimizing Activity of CoS ₂ for Hydrogen Evolution Reaction through the Synergic Effect of N Dopants and S Vacancies. ACS Energy Letters, 2017, 2, 1022-1028.	8.8	229
18	Shifting Oxygen Charge Towards Octahedral Metal: A Way to Promote Water Oxidation on Cobalt Spinel Oxides. Angewandte Chemie - International Edition, 2019, 58, 6042-6047.	7.2	226

#	Article	IF	CITATIONS
19	Mastering Surface Reconstruction of Metastable Spinel Oxides for Better Water Oxidation. Advanced Materials, 2019, 31, e1807898.	11.1	215
20	Atomically Dispersed Cobalt Trifunctional Electrocatalysts with Tailored Coordination Environment for Flexible Rechargeable Zn–Air Battery and Selfâ€Driven Water Splitting. Advanced Energy Materials, 2020, 10, 2002896.	10.2	210
21	High-performance flexible quasi-solid-state zinc-ion batteries with layer-expanded vanadium oxide cathode and zinc/stainless steel mesh composite anode. Nano Energy, 2019, 62, 94-102.	8.2	209
22	Boosting Electrochemical CO ₂ Reduction on Metal–Organic Frameworks via Ligand Doping. Angewandte Chemie - International Edition, 2019, 58, 4041-4045.	7.2	199
23	Efficient Hydrogen Evolution of Oxidized Niâ€N ₃ Defective Sites for Alkaline Freshwater and Seawater Electrolysis. Advanced Materials, 2021, 33, e2003846.	11.1	198
24	Mechanistic analysis of multiple processes controlling solar-driven H2O2 synthesis using engineered polymeric carbon nitride. Nature Communications, 2021, 12, 3701.	5.8	175
25	Synthesis of orthogonally assembled 3D cross-stacked metal oxide semiconducting nanowires. Nature Materials, 2020, 19, 203-211.	13.3	172
26	Enhanced Catalysis of the Electrochemical Oxygen Evolution Reaction by Iron(III) Ions Adsorbed on Amorphous Cobalt Oxide. ACS Catalysis, 2018, 8, 807-814.	5.5	163
27	Crystal Phase and Architecture Engineering of Lotusâ€Thalamusâ€Shaped Ptâ€Ni Anisotropic Superstructures for Highly Efficient Electrochemical Hydrogen Evolution. Advanced Materials, 2018, 30, e1801741.	11.1	163
28	Tuning the Catalytic Preference of Ruthenium Catalysts for Nitrogen Reduction by Atomic Dispersion. Advanced Functional Materials, 2020, 30, 1905665.	7.8	159
29	Single-Atom Coated Separator for Robust Lithium–Sulfur Batteries. ACS Applied Materials & Interfaces, 2019, 11, 25147-25154.	4.0	152
30	Engineering High‧pin State Cobalt Cations in Spinel Zinc Cobalt Oxide for Spin Channel Propagation and Active Site Enhancement in Water Oxidation. Angewandte Chemie - International Edition, 2021, 60, 14536-14544.	7.2	149
31	Atomic engineering of high-density isolated Co atoms on graphene with proximal-atom controlled reaction selectivity. Nature Communications, 2018, 9, 3197.	5.8	146
32	Enhanced performance and selectivity of CO2 methanation over phyllosilicate structure derived Ni-Mg/SBA-15 catalysts. Applied Catalysis B: Environmental, 2021, 282, 119564.	10.8	145
33	Linkage Effect in the Heterogenization of Cobalt Complexes by Doped Graphene for Electrocatalytic CO ₂ Reduction. Angewandte Chemie - International Edition, 2019, 58, 13532-13539.	7.2	143
34	Superexchange Effects on Oxygen Reduction Activity of Edgeâ€Sharing [Co <i>_x</i> Mn _{1â~'} <i>_x</i> O ₆] Octahedra in Spinel Oxide. Advanced Materials, 2018, 30, 1705407.	11.1	142
35	Enhanced Electrocatalytic Hydrogen Evolution Activity in Single-Atom Pt-Decorated VS ₂ Nanosheets. ACS Nano, 2020, 14, 5600-5608.	7.3	135
36	Dielectric Polarization in Inverse Spinel‣tructured Mg ₂ TiO ₄ Coating to Suppress Oxygen Evolution of Liâ€Rich Cathode Materials. Advanced Materials, 2020, 32, e2000496.	11.1	134

Sніво Xi

#	Article	IF	CITATIONS
37	Sizeâ€Dependent Activity and Selectivity of Atomicâ€Level Copper Nanoclusters during CO/CO ₂ Electroreduction. Angewandte Chemie - International Edition, 2021, 60, 466-472.	7.2	130
38	Anodic Oxidation Enabled Cation Leaching for Promoting Surface Reconstruction in Water Oxidation. Angewandte Chemie - International Edition, 2021, 60, 7418-7425.	7.2	130
39	High-performance NaFePO ₄ formed by aqueous ion-exchange and its mechanism for advanced sodium ion batteries. Journal of Materials Chemistry A, 2016, 4, 4882-4892.	5.2	129
40	Engineering Local and Global Structures of Single Co Atoms for a Superior Oxygen Reduction Reaction. ACS Catalysis, 2020, 10, 5862-5870.	5.5	126
41	XAFCA: a new XAFS beamline for catalysis research. Journal of Synchrotron Radiation, 2015, 22, 839-843.	1.0	125
42	Lowering Charge Transfer Barrier of LiMn ₂ O ₄ via Nickel Surface Doping To Enhance Li ⁺ Intercalation Kinetics at Subzero Temperatures. Journal of the American Chemical Society, 2019, 141, 14038-14042.	6.6	125
43	Constructing an Adaptive Heterojunction as a Highly Active Catalyst for the Oxygen Evolution Reaction. Advanced Materials, 2020, 32, e2001292.	11.1	122
44	Porous NiCo2S4/FeOOH nanowire arrays with rich sulfide/hydroxide interfaces enable high OER activity. Nano Energy, 2020, 78, 105230.	8.2	121
45	Atomically Dispersed Indium Sites for Selective CO ₂ Electroreduction to Formic Acid. ACS Nano, 2021, 15, 5671-5678.	7.3	121
46	Metastable 1T′-phase group VIB transition metal dichalcogenide crystals. Nature Materials, 2021, 20, 1113-1120.	13.3	119
47	Materializing efficient methanol oxidation via electron delocalization in nickel hydroxide nanoribbon. Nature Communications, 2020, 11, 4647.	5.8	117
48	Atomically-precise dopant-controlled single cluster catalysis for electrochemical nitrogen reduction. Nature Communications, 2020, 11, 4389.	5.8	110
49	Long-chain hydrocarbons by CO2 electroreduction using polarized nickel catalysts. Nature Catalysis, 2022, 5, 545-554.	16.1	107
50	Antiferromagnetic Inverse Spinel Oxide LiCoVO ₄ with Spinâ€Polarized Channels for Water Oxidation. Advanced Materials, 2020, 32, e1907976.	11.1	106
51	Preparation of 1T′-Phase ReS _{2<i>x</i>} Se _{2(1-<i>x</i>)} (<i>x</i> = 0–1) Nanodots for Highly Efficient Electrocatalytic Hydrogen Evolution Reaction. Journal of the American Chemical Society, 2018, 140, 8563-8568.	6.6	104
52	Bifunctional Oxygen Electrocatalyst of Mesoporous Ni/NiO Nanosheets for Flexible Rechargeable Zn–Air Batteries. Nano-Micro Letters, 2020, 12, 68.	14.4	103
53	Role of lattice oxygen in methane activation on Ni-phyllosilicate@Ce1-xZrxO2 core-shell catalyst for methane dry reforming: Zr doping effect, mechanism, and kinetic study. Applied Catalysis B: Environmental, 2021, 290, 119998.	10.8	100
54	Modulating Pt-O-Pt atomic clusters with isolated cobalt atoms for enhanced hydrogen evolution catalysis. Nature Communications, 2022, 13, 2430.	5.8	98

Sніво Xi

#	Article	IF	CITATIONS
55	Restructuring highly electron-deficient metal-metal oxides for boosting stability in acidic oxygen evolution reaction. Nature Communications, 2021, 12, 5676.	5.8	92
56	Phaseâ€Junction Electrocatalysts towards Enhanced Hydrogen Evolution Reaction in Alkaline Media. Angewandte Chemie - International Edition, 2021, 60, 259-267.	7.2	91
57	Constructing Atomic Heterometallic Sites in Ultrathin Nickel-Incorporated Cobalt Phosphide Nanosheets via a Boron-Assisted Strategy for Highly Efficient Water Splitting. Nano Letters, 2021, 21, 823-832.	4.5	91
58	Identifying the Origin and Contribution of Surface Storage in TiO ₂ (B) Nanotube Electrode by In Situ Dynamic Valence State Monitoring. Advanced Materials, 2018, 30, e1802200.	11.1	90
59	An electron deficiency strategy for enhancing hydrogen evolution on CoP nano-electrocatalysts. Nano Energy, 2018, 50, 273-280.	8.2	89
60	Dehydrationâ€Triggered Ionic Channel Engineering in Potassium Niobate for Li/Kâ€lon Storage. Advanced Materials, 2020, 32, e2000380.	11.1	85
61	Ordered clustering of single atomic Te vacancies in atomically thin PtTe2 promotes hydrogen evolution catalysis. Nature Communications, 2021, 12, 2351.	5.8	83
62	lsolated FeN ₄ Sites for Efficient Electrocatalytic CO ₂ Reduction. Advanced Science, 2020, 7, 2001545.	5.6	81
63	Effect of Partial Fe Substitution in La _{0.9} Sr _{0.1} NiO ₃ Perovskite-Derived Catalysts on the Reaction Mechanism of Methane Dry Reforming. ACS Catalysis, 2020, 10, 12466-12486.	5.5	80
64	Tuning the Electronic Structure of NiO via Li Doping for the Fast Oxygen Evolution Reaction. Chemistry of Materials, 2019, 31, 419-428.	3.2	78
65	Strain stabilized nickel hydroxide nanoribbons for efficient water splitting. Energy and Environmental Science, 2020, 13, 229-237.	15.6	78
66	Heterostructure Design in Bimetallic Phthalocyanine Boosts Oxygen Reduction Reaction Activity and Durability. Advanced Functional Materials, 2020, 30, 2005000.	7.8	78
67	LaNiO3 as a precursor of Ni/La2O3 for reverse water-gas shift in DBD plasma: Effect of calcination temperature. Energy Conversion and Management, 2020, 206, 112475.	4.4	74
68	Plasma-induced on-surface sulfur vacancies in NiCo ₂ S ₄ enhance the energy storage performance of supercapatteries. Journal of Materials Chemistry A, 2020, 8, 9278-9291.	5.2	73
69	Polyoxometalate immobilized in MIL-101(Cr) as an efficient catalyst for water oxidation. Applied Catalysis A: General, 2016, 521, 83-89.	2.2	70
70	Shifting Oxygen Charge Towards Octahedral Metal: A Way to Promote Water Oxidation on Cobalt Spinel Oxides. Angewandte Chemie, 2019, 131, 6103-6108.	1.6	69
71	Universal Approach to Fabricating Graphene-Supported Single-Atom Catalysts from Doped ZnO Solid Solutions. ACS Central Science, 2020, 6, 1431-1440.	5.3	69
72	Identifying Influential Parameters of Octahedrally Coordinated Cations in Spinel ZnMn _{<i>x</i>} Co _{2–<i>x</i>} O ₄ Oxides for the Oxidation Reaction. ACS Catalysis, 2018, 8, 8568-8577.	5.5	68

#	Article	lF	CITATIONS
73	Activation of Surface Oxygen Sites in a Cobalt-Based Perovskite Model Catalyst for CO Oxidation. Journal of Physical Chemistry Letters, 2018, 9, 4146-4154.	2.1	67
74	Immediate hydroxylation of arenes to phenols via V-containing all-silica ZSM-22 zeolite triggered non-radical mechanism. Nature Communications, 2018, 9, 2931.	5.8	66
75	Metal–Oxygen Hybridization Determined Activity in Spinel-Based Oxygen Evolution Catalysts: A Case Study of ZnFe _{2–<i>x</i>} Cr _{<i>x</i>} O ₄ . Chemistry of Materials, 2018, 30, 6839-6848.	3.2	65
76	Axial Modification of Cobalt Complexes on Heterogeneous Surface with Enhanced Electron Transfer for Carbon Dioxide Reduction. Angewandte Chemie - International Edition, 2020, 59, 19162-19167.	7.2	64
77	Redox Targeting-Based Vanadium Redox-Flow Battery. ACS Energy Letters, 2019, 4, 3028-3035.	8.8	63
78	Approaching the Lithiation Limit of MoS ₂ While Maintaining Its Layered Crystalline Structure to Improve Lithium Storage. Angewandte Chemie - International Edition, 2019, 58, 3521-3526.	7.2	62
79	Low temperature catalytic reverse water-gas shift reaction over perovskite catalysts in DBD plasma. Applied Catalysis B: Environmental, 2020, 265, 118573.	10.8	62
80	Cobalt Singleâ€Atomâ€Intercalated Molybdenum Disulfide for Sulfide Oxidation with Exceptional Chemoselectivity. Advanced Materials, 2020, 32, e1906437.	11.1	62
81	Hybrid MOF-808-Tb nanospheres for highly sensitive and selective detection of acetone vapor and Fe ³⁺ in aqueous solution. Chemical Communications, 2019, 55, 4727-4730.	2.2	61
82	Highly Dispersed Ni/Silica by Carbonization–Calcination of a Chelated Precursor for Coke-Free Dry Reforming of Methane. ACS Applied Energy Materials, 2020, 3, 7719-7735.	2.5	60
83	Site-selective alkene borylation enabled by synergistic hydrometallation and borometallation. Nature Catalysis, 2020, 3, 585-592.	16.1	60
84	Revealing the Dominant Chemistry for Oxygen Reduction Reaction on Small Oxide Nanoparticles. ACS Catalysis, 2018, 8, 673-677.	5.5	58
85	Mixed Copper/Copperâ€Oxide Anchored Mesoporous Fullerene Nanohybrids as Superior Electrocatalysts toward Oxygen Reduction Reaction. Small, 2020, 16, e1903937.	5.2	58
86	β-FeOOH: An Earth-Abundant High-Capacity Negative Electrode Material for Sodium-Ion Batteries. Chemistry of Materials, 2015, 27, 5340-5348.	3.2	57
87	Metal–organic framework immobilized cobalt oxide nanoparticles for efficient photocatalytic water oxidation. Journal of Materials Chemistry A, 2015, 3, 20607-20613.	5.2	57
88	Encapsulating porous SnO ₂ into a hybrid nanocarbon matrix for long lifetime Li storage. Journal of Materials Chemistry A, 2017, 5, 25609-25617.	5.2	57
89	Superior Lithium Storage Properties of βâ€FeOOH. Advanced Energy Materials, 2015, 5, 1401517.	10.2	56
90	Degree of Geometric Tilting Determines the Activity of FeO ₆ Octahedra for Water Oxidation. Chemistry of Materials, 2018, 30, 4313-4320.	3.2	54

#	Article	IF	CITATIONS
91	Interfacial Lattice‧trainâ€Driven Generation of Oxygen Vacancies in an Aerobicâ€Annealed TiO ₂ (B) Electrode. Advanced Materials, 2019, 31, e1906156.	11.1	53
92	Cu and Co nanoparticle-Co-decorated N-doped graphene nanosheets: a high efficiency bifunctional electrocatalyst for rechargeable Zn–air batteries. Journal of Materials Chemistry A, 2019, 7, 12851-12858.	5.2	50
93	Electrochemical oxidation of C3 saturated alcohols on Co3O4 in alkaline. Electrochimica Acta, 2017, 228, 183-194.	2.6	45
94	Mesoporous 3D/2D NiCoP/g-C ₃ N ₄ Heterostructure with Dual Co–N and Ni–N Bonding States for Boosting Photocatalytic H ₂ Production Activity and Stability. ACS Sustainable Chemistry and Engineering, 2020, 8, 12934-12943.	3.2	45
95	Zr–Ce-incorporated Ni/SBA-15 catalyst for high-temperature water gas shift reaction: Methane suppression by incorporated Zr and Ce. Journal of Catalysis, 2020, 387, 47-61.	3.1	44
96	Rational Design and Synthesis of Hierarchical Porous Mn–N–C Nanoparticles with Atomically Dispersed MnN <i>_x</i> Moieties for Highly Efficient Oxygen Reduction Reaction. ACS Sustainable Chemistry and Engineering, 2020, 8, 9367-9376.	3.2	43
97	In-situ studies of oxidation/reduction of copper in Cu-CHA SCR catalysts: Comparison of fresh and SO2-poisoned catalysts. Applied Catalysis B: Environmental, 2020, 269, 118722.	10.8	42
98	Promoting Dinuclearâ€Type Catalysis in Cu ₁ –C ₃ N ₄ Singleâ€Atom Catalysts. Advanced Materials, 2022, 34, .	11.1	42
99	Bifunctional Electrocatalytic Activity of Nitrogen-Doped NiO Nanosheets for Rechargeable Zinc–Air Batteries. ACS Applied Materials & Interfaces, 2019, 11, 30865-30871.	4.0	41
100	Facile synthesis of copper nanoparticles in glycerol at room temperature: formation mechanism. RSC Advances, 2015, 5, 24544-24549.	1.7	40
101	Nitrogen-Doped Cobalt Phosphide for Enhanced Hydrogen Evolution Activity. ACS Applied Materials & Interfaces, 2019, 11, 17359-17367.	4.0	40
102	Promoted Glycerol Oxidation Reaction in an Interface onfined Hierarchically Structured Catalyst. Advanced Materials, 2019, 31, e1804763.	11.1	40
103	FeN _x and γ-Fe ₂ O ₃ co-functionalized hollow graphitic carbon nanofibers for efficient oxygen reduction in an alkaline medium. Journal of Materials Chemistry A, 2020, 8, 6076-6082.	5.2	40
104	Facilitating the Deprotonation of OH to O through Fe ⁴⁺ â€Induced States in Perovskite LaNiO ₃ Enables a Fast Oxygen Evolution Reaction. Small, 2021, 17, e2006930.	5.2	40
105	Developing an O3 type layered oxide cathode and its application in 18650 commercial type Na-ion batteries. Journal of Materials Chemistry A, 2019, 7, 25944-25960.	5.2	39
106	Enhancing cycling stability of transition metal-based layered double hydroxides through a self-sacrificial strategy for hybrid supercapacitors. Electrochimica Acta, 2020, 334, 135586.	2.6	39
107	Iron Single Atom Catalyzed Quinoline Synthesis. Advanced Materials, 2021, 33, e2101382.	11.1	39
108	Spinel Manganese Ferrites for Oxygen Electrocatalysis: Effect of Mn Valency and Occupation Site. Electrocatalysis, 2018, 9, 287-292.	1.5	38

#	Article	IF	CITATIONS
109	Unraveling the Formation of Amorphous MoS ₂ Nanograins during the Electrochemical Delithiation Process. Advanced Functional Materials, 2019, 29, 1904843.	7.8	38
110	Na ₃ V ₂ (PO ₄) ₃ as the Sole Solid Energy Storage Material for Redox Flow Sodiumâ€lon Battery. Advanced Energy Materials, 2019, 9, 1901188.	10.2	38
111	Catalytically Influential Features in Transition Metal Oxides. ACS Catalysis, 2021, 11, 13947-13954.	5.5	38
112	Origin of electronic structure dependent activity of spinel ZnNixCo2-xO4 oxides for complete methane oxidation. Applied Catalysis B: Environmental, 2019, 256, 117844.	10.8	35
113	Divergent Chemistry Paths for 3D and 1D Metallo ovalent Organic Frameworks (COFs). Angewandte Chemie - International Edition, 2020, 59, 11527-11532.	7.2	35
114	Mesoporous amorphous Al ₂ O ₃ /crystalline WO ₃ heterophase hybrids for electrocatalysis and gas sensing applications. Journal of Materials Chemistry A, 2019, 7, 21874-21883.	5.2	34
115	Deciphering NH ₃ Adsorption Kinetics in Ternary Ni–Cu–Fe Oxyhydroxide toward Efficient Ammonia Oxidation Reaction. Small, 2021, 17, e2005616.	5.2	34
116	Unexpected discovery of magnesium-vanadium spinel oxide containing extractable Mg2+ as a high-capacity cathode material for magnesium ion batteries. Chemical Engineering Journal, 2021, 405, 127005.	6.6	34
117	Current-induced self-switching of perpendicular magnetization in CoPt single layer. Nature Communications, 2022, 13, .	5.8	33
118	Trimetal atoms confined in openly accessible nitrogen-doped carbon constructs for an efficient ORR. Journal of Materials Chemistry A, 2020, 8, 17266-17275.	5.2	32
119	The interplay between the suprafacial and intrafacial mechanisms for complete methane oxidation on substituted LaCoO3 perovskite oxides. Journal of Catalysis, 2020, 390, 1-11.	3.1	32
120	Expedient synthesis of <i>E</i> -hydrazone esters and 1 <i>H</i> -indazole scaffolds through heterogeneous single-atom platinum catalysis. Science Advances, 2019, 5, eaay1537.	4.7	31
121	Cation-synergy stabilizing anion redox of Chevrel phase Mo6S8 in aluminum ion battery. Energy Storage Materials, 2021, 37, 87-93.	9.5	31
122	Four-state memory based on a giant and non-volatile converse magnetoelectric effect in FeAl/PIN-PMN-PT structure. Scientific Reports, 2016, 6, 30002.	1.6	29
123	On the synthesis and performance of hierarchical nanoporous TS-1 catalysts. Microporous and Mesoporous Materials, 2017, 244, 83-92.	2.2	29
124	Activation of Copper Species on Carbon Nitride for Enhanced Activity in the Arylation of Amines. ACS Catalysis, 2020, 10, 11069-11080.	5.5	29
125	Elucidating the Strain–Vacancy–Activity Relationship on Structurally Deformed Co@CoO Nanosheets for Aqueous Phase Reforming of Formaldehyde. Small, 2021, 17, e2102970.	5.2	29
126	Facile synthesis of Mn2.1V0.9O4/rGO: A novel high-rate anode material for lithium-ion batteries. Journal of Power Sources, 2019, 426, 197-204.	4.0	28

#	Article	IF	CITATIONS
127	Selective conversion of lactic acid to acrylic acid over alkali and alkaline-earth metal co-modified NaY zeolites. Catalysis Science and Technology, 2017, 7, 6101-6111.	2.1	26
128	Incorporating MoO ₃ Patches into a Ni Oxyhydroxide Nanosheet Boosts the Electrocatalytic Oxygen Evolution Reaction. ACS Applied Materials & Interfaces, 2021, 13, 26064-26073.	4.0	26
129	Directly synthesized V-containing BEA zeolite: Acid-oxidation bifunctional catalyst enhancing C-alkylation selectivity in liquid-phase methylation of phenol. Chemical Engineering Journal, 2017, 328, 1031-1042.	6.6	25
130	Single Solid Precursor-Derived Three-Dimensional Nanowire Networks of CuZn-Silicate for CO ₂ Hydrogenation to Methanol. ACS Catalysis, 2022, 12, 5750-5765.	5.5	24
131	Influence of Surface Formate Species on Methane Selectivity for Carbon Dioxide Methanation over Nickel Hydroxyapatite Catalyst. ChemCatChem, 2020, 12, 6410-6419.	1.8	23
132	Addressing the quantitative conversion bottleneck in single-atom catalysis. Nature Communications, 2022, 13, 2807.	5.8	23
133	Introducing Na-sufficient P3-Na _{0.9} Fe _{0.5} Mn _{0.5} O ₂ as a cathode material for Na-ion batteries. Chemical Communications, 2020, 56, 10686-10689.	2.2	22
134	Colossal Magnetization and Giant Coercivity in Ion-Implanted (Nb and Co) MoS ₂ Crystals. ACS Applied Materials & Interfaces, 2020, 12, 58140-58148.	4.0	22
135	Impeding Catalyst Sulfur Poisoning in Aqueous Solution by Metal–Organic Framework Composites. Small Methods, 2020, 4, 1900890.	4.6	22
136	Operando Investigation of Mn ₃ O _{4+δ} Co-catalyst on Fe ₂ O ₃ Photoanode: Manganese-Valency-Determined Enhancement at Varied Potentials. ACS Applied Energy Materials, 2018, 1, 814-821.	2.5	21
137	Revamping SiO ₂ Spheres by Core–Shell Porosity Endowment to Construct a Mazelike Nanoreactor for Enhanced Catalysis in CO ₂ Hydrogenation to Methanol. Advanced Functional Materials, 2021, 31, 2102896.	7.8	21
138	Regeneration of sulfur-poisoned Cu-SSZ-13 catalysts: Copper speciation and catalytic performance evaluation. Applied Catalysis B: Environmental, 2021, 299, 120626.	10.8	21
139	CO ₂ Hydrogenation to Methanol over Partially Reduced Cu-SiO _{2P} Catalysts: The Crucial Role of Hydroxyls for Methanol Selectivity. ACS Applied Energy Materials, 2021, 4, 12149-12162.	2.5	21
140	Structure Sensitivity and Evolution of Nickel-Bearing Nitrogen-Doped Carbons in the Electrochemical Reduction of CO ₂ . ACS Catalysis, 2020, 10, 3444-3454.	5.5	20
141	Differences in oxidation-reduction kinetics and mobility of Cu species in fresh and SO2-poisoned Cu-SSZ-13 catalysts. Applied Catalysis B: Environmental, 2021, 284, 119756.	10.8	20
142	Chemical design and synthesis of superior single-atom electrocatalysts <i>via in situ</i> polymerization. Journal of Materials Chemistry A, 2020, 8, 17683-17690.	5.2	19
143	αâ€Ni(OH) ₂ Originated from Electroâ€Oxidation of NiSe ₂ Supported by Carbon Nanoarray on Carbon Cloth for Efficient Water Oxidation. Small, 2019, 15, e1902222.	5.2	18
144	Molecular engineered palladium single atom catalysts with an M-C ₁ N ₃ subunit for Suzuki coupling. Journal of Materials Chemistry A, 2021, 9, 11427-11432.	5.2	18

#	Article	IF	CITATIONS
145	Dynamic structural transformation induced by defects in nano-rod FeOOH during electrochemical water splitting. Journal of Materials Chemistry A, 2022, 10, 602-610.	5.2	18
146	Synthesis of Mesoporous Copper Aluminosilicate Hollow Spheres for Oxidation Reactions. ACS Applied Materials & Interfaces, 2020, 12, 23060-23075.	4.0	17
147	Origin of Magnetism in Hydrothermally Aged 2-Line Ferrihydrite Suspensions. Environmental Science & Technology, 2017, 51, 2643-2651.	4.6	16
148	Hybrid Nanomaterials with Single-Site Catalysts by Spatially Controllable Immobilization of Nickel Complexes <i>via</i> Photoclick Chemistry for Alkene Epoxidation. ACS Nano, 2018, 12, 5903-5912.	7.3	16
149	Sizeâ€Dependent Activity and Selectivity of Atomic‣evel Copper Nanoclusters during CO/CO ₂ Electroreduction. Angewandte Chemie, 2021, 133, 470-476.	1.6	16
150	Room-Temperature Ferromagnetism in Fe/Sn-Codoped In ₂ O ₃ Powders and Thin Films. Chinese Physics Letters, 2013, 30, 047501.	1.3	14
151	A symbiotic hetero-nanocomposite that stabilizes unprecedented CaCl ₂ -type TiO ₂ for enhanced solar-driven hydrogen evolution reaction. Chemical Science, 2019, 10, 8323-8330.	3.7	14
152	Direct Pyrolysis of a Manganeseâ€īriazolate Metal–Organic Framework into Air‣table Manganese Nitride Nanoparticles. Advanced Science, 2021, 8, 2003212.	5.6	13
153	Anion vacancy-mediated ferromagnetism in atomic-thick Ni3N nanosheets. Applied Physics Letters, 2017, 111, .	1.5	11
154	Origin of giant electric-field-induced strain in faulted alkali niobate films. Nature Communications, 2022, 13, .	5.8	11
155	Divergent Chemistry Paths for 3D and 1D Metallo ovalent Organic Frameworks (COFs). Angewandte Chemie, 2020, 132, 11624-11629.	1.6	10
156	Probing the Oxidation/Reduction Dynamics of Fresh and P-, Na-, and K-Contaminated Pt/Pd/Al ₂ O ₃ Diesel Oxidation Catalysts by STEM, TPR, and in Situ XANES. Journal of Physical Chemistry C, 2020, 124, 2945-2952.	1.5	10
157	Heteroatomic Znâ€MWW Zeolite Developed for Catalytic Dehydrogenation Reactions: A Combined Experimental and DFT Study. ChemCatChem, 2018, 10, 3078-3085.	1.8	8
158	Ti1-Sn O2 nanofilms: Layer-by-layer deposition with extended Sn solubility and characterization. Applied Surface Science, 2018, 428, 710-717.	3.1	7
159	Accelerated Formation Kinetics of a Multicomponent Metal–Organic Framework Derived from Preferential Site Occupancy. Inorganic Chemistry, 2020, 59, 9350-9355.	1.9	7
160	Impact of Biodiesel-Based Phosphorus and Sulfur on Copper Speciation of Cu-SSZ-13 Catalysts: XAFS Scanning during H ₂ -TPR. Journal of Physical Chemistry C, 2022, 126, 3385-3396.	1.5	7
161	Determination of the calcium species in coal chars by Ca K-edge XANES analysis. Chinese Physics C, 2013, 37, 028003.	1.5	6
162	Mussel-inspired facile synthesis of Fe/Co-polydopamine complex nanospheres: complexation mechanism and application of the carbonized hybrid nanospheres as an efficient bifunctional electrocatalyst. New Journal of Chemistry, 2018, 42, 19494-19504.	1.4	6

Sніво Xi

#	Article	IF	CITATIONS
163	Breaking the Stoichiometric Limit in Oxygen-Carrying Capacity of Fe-Based Oxygen Carriers for Chemical Looping Combustion using the Mg-Fe-O Solid Solution System. ACS Sustainable Chemistry and Engineering, 2022, 10, 7242-7252.	3.2	6
164	General method for automatic on-line beamline optimization based on genetic algorithm. Journal of Synchrotron Radiation, 2015, 22, 661-665.	1.0	5
165	Measurement of the polarization for soft X-ray magnetic circular dichroism at the BSRF beamline 4B7B. Chinese Physics C, 2013, 37, 018001.	1.5	4
166	Dual catalyst system for selective vinyl chloride production <i>via</i> ethene oxychlorination. Catalysis Science and Technology, 2020, 10, 560-575.	2.1	4
167	Unravelling uniaxial strain effects on electronic correlations, hybridization and bonding in transition metal oxides. Acta Materialia, 2019, 164, 618-626.	3.8	3
168	Bismuth ion battery – A new member in trivalent battery technology. Energy Storage Materials, 2020, 25, 100-104.	9.5	3
169	Ultralow magnetic damping of a common metallic ferromagnetic film. Science Advances, 2021, 7, .	4.7	3
170	Soft X-ray magmeto-optical Faraday rotation measurements with the multilayer polarizer. Wuli Xuebao/Acta Physica Sinica, 2008, 57, 2860.	0.2	3
171	Origin of Ferromagnetism in Zn 1â~' x Co x O Thin Films: Evidences Provided by Hard and Soft X-Ray Absorption Spectroscopy. Chinese Physics Letters, 2012, 29, 127804.	1.3	2
172	<i>Al-BL</i> 1.0: a program for automatic on-line beamline optimization using the evolutionary algorithm. Journal of Synchrotron Radiation, 2017, 24, 367-373.	1.0	2
173	Electronic and Geometric Structures of Rechargeable Lithium Manganese Sulfate Li ₂ Mn(SO ₄) ₂ Cathode. ACS Omega, 2019, 4, 11338-11345.	1.6	2
174	Selective control of magnetism in FeAl/PIN-PMN-PT using an electric field. Applied Physics Letters, 2019, 114, .	1.5	2
175	Insights into sulfur poisoning and regeneration of Cu-SSZ-13 catalysts: in situ Cu and S K-edge XAS studies. Catalysis Science and Technology, 2021, 11, 5619-5632.	2.1	2
176	Catalytically active atomically thin cuprate with periodic Cu single sites. National Science Review, 2023, 10, .	4.6	2
177	Upgrade of beamline 3W1B at Beijing Synchrotron Radiation Facility. Chinese Physics C, 2013, 37, 058001.	1.5	1
178	An analytical model for the polarization of synchrotron radiation in a soft X-ray region. Chinese Physics C, 2013, 37, 038002.	1.5	1
179	Cyclic structural ordering induced by high energy ball milling in a Fe2.1Cr0.9Al magnetocaloric alloy. Journal of Magnetism and Magnetic Materials, 2019, 474, 528-536.	1.0	1
180	Performance of a polarizer using synthetic mica crystal in the 12–25 nm wavelength range. Chinese Physics C, 2011, 35, 509-513.	1.5	0

#	Article	IF	CITATIONS
181	X-Ray Magnetic Linear Dichroism of Co ₃₅ Fe ₆₅ Alloy Films Annealed with and without Oxygen Gas. Chinese Physics Letters, 2013, 30, 107501.	1.3	0